

Concentration Dependence of Frenkel-Pair-Defect Annealing in Electron-Irradiated Ta and Nb†

SVERRE MYHRA* AND JOHN W. DEFORD

Department of Physics, University of Utah, Salt Lake City, Utah 84112

(Received 19 May 1969)

The present work is an investigation into the dose dependence of the annealing spectra of Ta and Nb from 15 to 285°K after bombardment with 2.2-MeV electrons. Ta and Nb samples were irradiated to different defect concentrations, then simultaneously annealed isochronally from 14.7 up to 285°K. In Ta, recovery peaks were observed at 23, 51, 65, 123, and 170°K. The position of the peak near 170°K is dose-dependent and shows the characteristics of a second-order reaction. In Nb, recovery peaks were observed at 26.5, 58, 95, and 135°K. The peak at 95°K is dose-dependent and follows second-order kinetics initially, with an apparent shift to higher order toward the end of the stage. A two-interstitial model seems to give the best fit to the data.

I. INTRODUCTION

WHILE a great effort has been made over the last 15 years to understand the effects of electron irradiation on the fcc metals, comparatively little has been done on the bcc metals. The group-V metals V, Nb, and Ta in particular have been given little consideration. Recent work by Burger *et al.*¹ and by El-Salam and DeFord² have outlined the annealing spectra for Ta and Nb, but have been inconclusive as far as determining the character of the observed sub-stages. Some very recent work by the Stuttgart group³ has provided further information and led to the proposal of a two-interstitial model for Ta. The available information concerning activation energies and order of kinetics for the observed annealing spectra, however, is preliminary or simply nonexistent. Therefore, the present work was undertaken in order to investigate the effect of concentration on the sub-stages from 15 up to 285°K in Nb and Ta.

II. EXPERIMENTAL

A. Cryostat

A cross-sectional view of the assembled cryostat is shown in Fig. 1. The liquid-helium vessel, the heat switch, and the sample holder are enclosed by a heat shield soldered to the liquid-nitrogen vessel, in order to reduce liquid-helium losses due to thermal radiation. A vacuum of 6×10^{-6} Torr or better was maintained. The heat switch, similar to one described by Magnuson,

Palmer, and Koehler,⁴ constitutes a variable heat leak, such that the temperature of the sample holder can be raised without causing a prohibitive helium loss. The sample holder, shown in Fig. 2, was machined from a solid copper rod and soldered to the bottom of the heat switch. It was designed to provide good thermal contact between the samples and the helium reservoir via the heat switch and, in addition, to form a well-defined beam window. A resistance heater coil was wound around the stem and controlled with a variable-output constant current supply. Electrical leads were brought from the sample holder region to liquid-helium temperature, then to liquid-nitrogen temperature, and finally through a serum-cap seal to a connector plug on top of the cryostat.

B. Sample Preparation and Mounting

Nb and Ta sample material in the form of 0.002-in.-diam wires having a stated nominal purity of 40 parts per million (ppm) were obtained from Materials Research Corporation. The estimate for nominal purity proved to be somewhat optimistic in that the resistance ratios $R_{295^\circ\text{K}}/R_{11^\circ\text{K}}$ for the received sample material were about 15 for both Nb and Ta.

To avoid cold-working the samples after they were annealed, potential leads of the same material as the respective sample were spot-welded in place at the start of the preparation process. These leads were spaced about 3/16 in. apart, defining the active sample length. The samples were then outgassed and annealed just below the melting points of the samples for several hours in a 10^{-10} -Torr vacuum. Resistance ratios $R_{295^\circ\text{K}}/R_{11.5^\circ\text{K}}$ after this procedure and mounting are shown in Table I for the samples used in the present experiment. The improvement is significant for Ta, while only slight for Nb.

The procedure for mounting the samples is shown in Fig. 3. Six samples were mounted in two layers on separate "sandwiches," such that a Nb sample was almost directly above a Ta sample or vice versa along

† Research supported by the U. S. Atomic Energy Commission, under Contract No. AT(11-1)1494.

* Based on a thesis submitted in partial fulfillment of the requirements for the Ph.D. degree at the University of Utah, Salt Lake City, Utah.

¹ G. Burger, K. Isebeck, R. Kerler, J. Völkl, H. Wenzel, H. H. Kuhlmann, and H. Schultz, *Phys. Letters* **20**, 470 (1966); **20**, 472 (1966).

² Ehab M. Abd El-Salam and J. W. DeFord, *Phys. Rev.* **161**, 600 (1967).

³ H. Hemmerich, D. Meissner, H. Schultz, and F. Walz, in *Proceedings of the Conference on Interstitials and Vacancies*, Jülich, Germany, 1968 (unpublished).

⁴ G. D. Magnuson, W. Palmer, and J. S. Koehler, *Phys. Rev.* **109**, 1990 (1958).

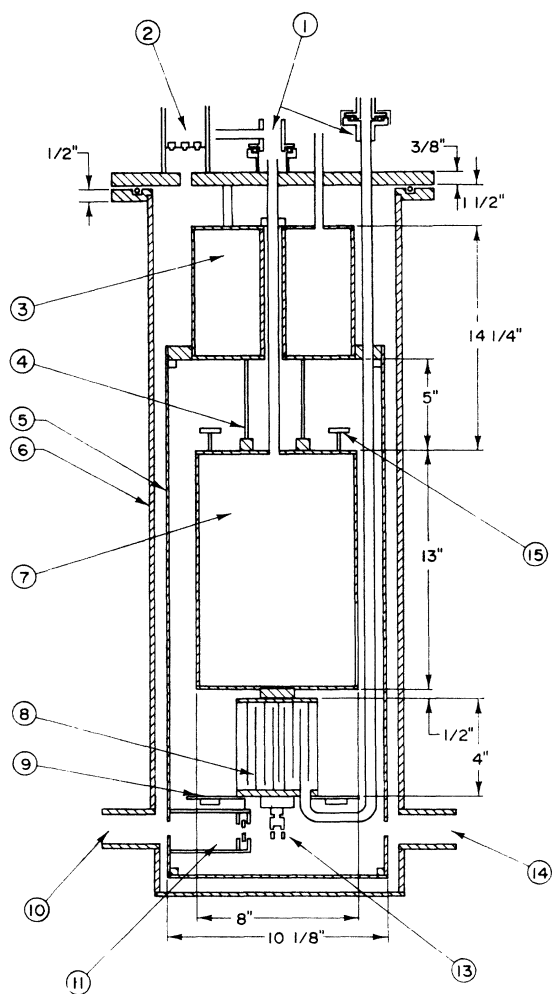


FIG. 1. Sectional view of cryostat: (1) quick connections, (2) serum cap feed-throughs, (3) liquid-nitrogen can, (4) support tube, (5) heat shield, (6) outer casing, (7) liquid-helium can, (8) heat switch, (9) terminal board, (10) entrance port, (11) slit system, (13) sample holder, (14) exit port, and (15) terminal board.

the beam direction. This facilitated the irradiation procedure since a pair of Nb and Ta samples could be bombarded independently of the two other pairs until the desired dose was achieved. The first step in the mounting procedure for a "sandwich" consisted in

TABLE I. Sample data.

Sample	Time outgassed (h)	$R_{295^{\circ}\text{K}}/R_{11.5^{\circ}\text{K}}$
VII Ta 12	6	258
IV Ta 13	3	142
VI Ta 14	3.5	206
II Ta 15 ^a	4 < <i>t</i> < 9	174
I Nb 13	3	26.3
III Nb 14	3.5	29.1
V Nb 15 ^a	4 < <i>t</i> < 9	25.6

^a Samples burned out overnight.

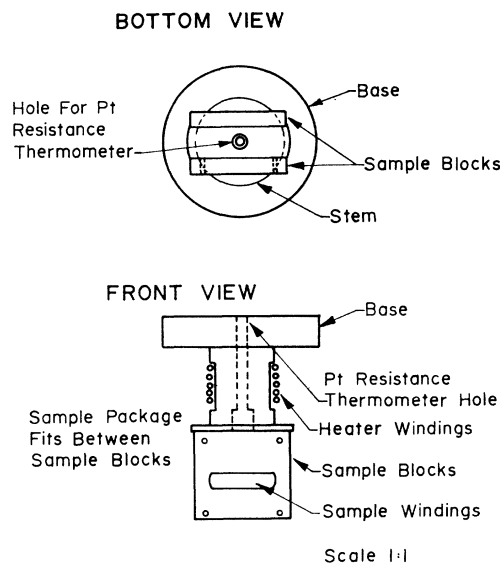


FIG. 2. The sample holder.

laying the three samples out on a 0.001-in. stainless-steel foil cut to the shape of the sample block. Two current and two potential leads per sample were then spot-welded to the foil. Subsequently, the foil was glued onto a Bakelite backing with Eastman 910 glue and was left to dry. Strips of foil were then cut away such that one current and two potential leads per sample were

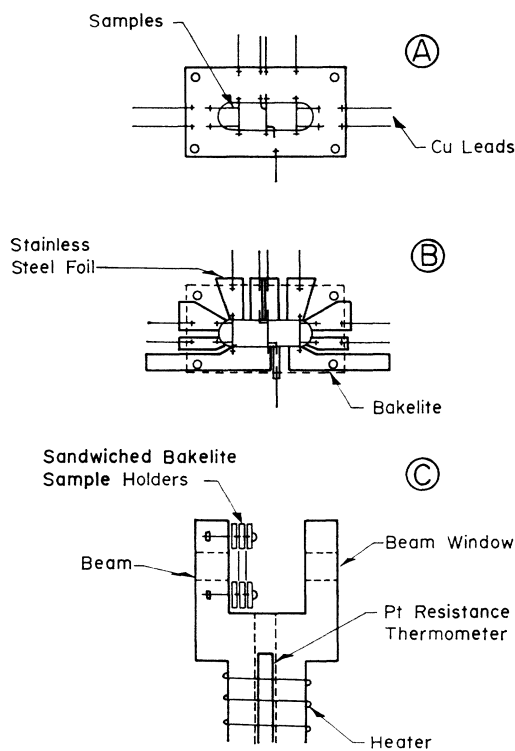


FIG. 3. Sample mounting procedure.

electrically insulated while one current lead per sample was left as a common lead. Next, copper leads were soldered to the appropriate pieces of foil and later connected to electrical leads running to the outside of the cryostat. The two "sandwiches" were glued together and slipped in between the two sample blocks. G. E. varnish 7031 was used to improve the thermal contact between the sample package and the sample holder. Finally, the common-current leads were soldered directly onto the sample block to further improve the thermal contact.

C. Resistance and Temperature Measurements

The resistance measurements were made with the standard Rubicon six-dial potentiometer arrangement. The six samples were connected to six independent constant-current supplies which were regulated to 1×10^{-4} . All data were taken using a 10-mA measuring current.

Temperature was monitored with a platinum resistance thermometer, calibrated by the National Bureau of Standards, embedded in the stem of the sample holder. The 10-mA thermometer current was also provided by a constant-current supply. Because of the large thermal inertia of the sample holder and a time-dependent temperature lag between the sample holder and the sample package during heating and cooling, the platinum resistance thermometer was supplemented with a dummy sample. The dummy sample, calibrated at thermal equilibrium with the platinum resistance thermometer, was used to measure the temperature of the sample package during nonequilibrium conditions like annealing.

D. Irradiation

The irradiation was done in the University of Utah 2.5-MeV Van de Graaff electron-accelerator facility. To ensure reasonable damage rates, the samples were bombarded with 2.2-MeV electrons. The beam current, $0.7\text{--}1.2 \mu\text{A}/\text{cm}^2$, caused a heating of the samples of about 2°K such that the irradiation was performed at approximately 14°K .

E. Isochronal Annealing

Isochronal anneals were made from 14.7 to 80.3°K in temperature increments that, on the average, were equal to 5% of the annealing temperature. After each anneal, resistance measurements were made at a base temperature of 11.9°K . The annealing pulse length was 10 min and heating and cooling times were generally less than 1 min for the last degree K. Temperature instability ($\Delta T_{\text{peak-to-peak}}$) during the annealing pulses was usually less than 0.08°K . From 82.3 up to 285°K , liquid nitrogen was substituted for liquid helium and a new base temperature was established at 78.0°K .

III. DAMAGE PRODUCTION

Damage production is discussed in Paper II. The results obtained in the present experiment are shown in Table II.

IV. RECOVERY

Curves showing the normalized recovery from 14.7 to 285°K for the five irradiated samples are presented in Figs. 4(a)–4(e) and in derivative form in Figs.

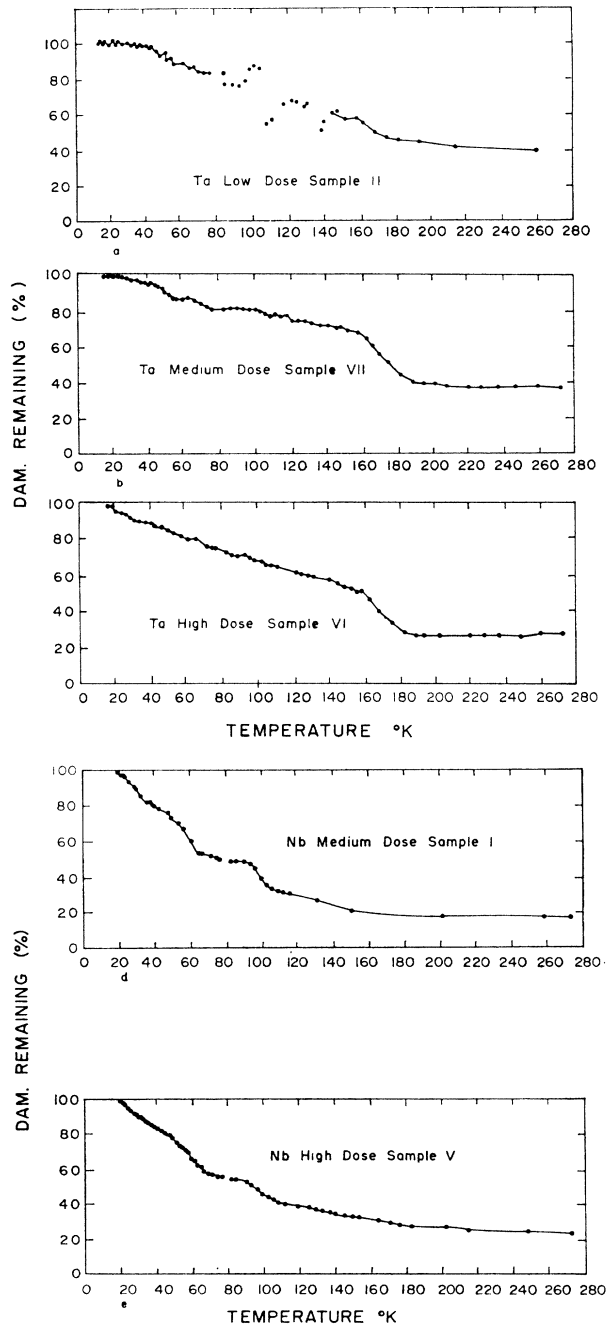


FIG. 4. (a)–(c) Isochronal annealing curves for Ta. (d)–(e) Isochronal annealing curves for Nb.

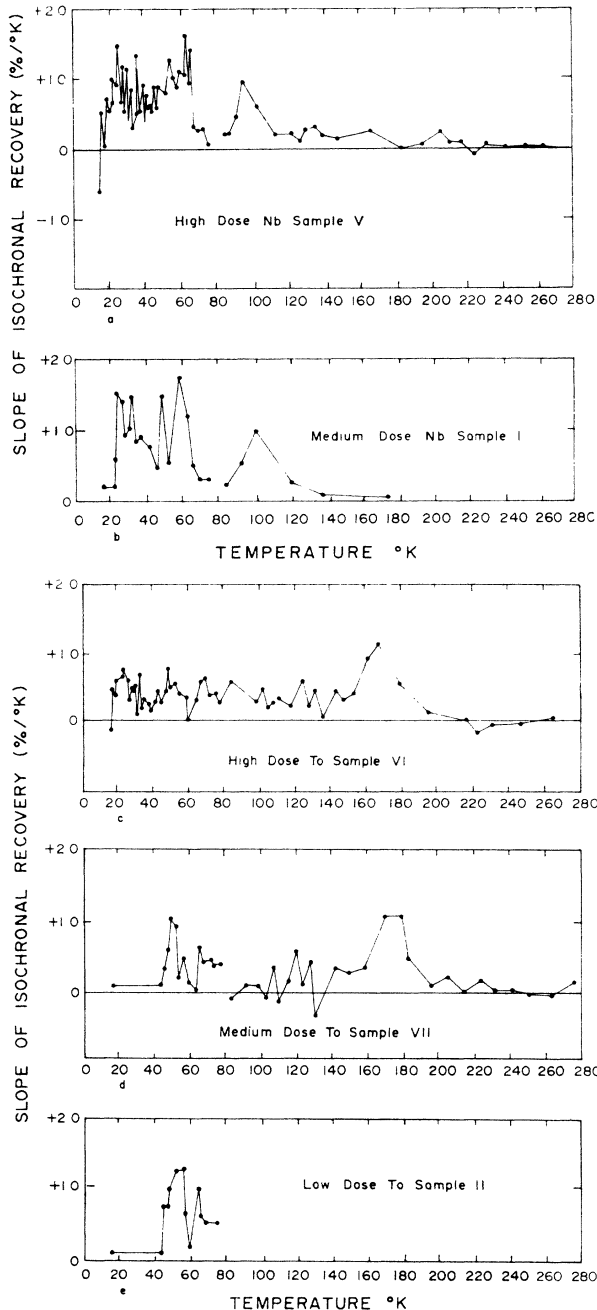


FIG. 5. (a)-(b) Slope of isochronal annealing curves for Nb. (c)-(e) Slope of isochronal annealing curves for Ta.

5(a)-5(e). Because of the limited experimental accuracy of the medium- and low-dose data, and of the liquid-nitrogen measurements, the temperature increments were increased in the analysis of this data in order to reduce the experimental scatter. Where the rate of annealing was below the experimental accuracy, the slope has been averaged over large temperature intervals. This is shown by straight horizontal lines in the derivative curves.

The slope diagrams for Ta reveal five substages centered at 23, 51, 65, 123, and 167°K. These are labeled as $II_A(Ta)$, $II_B(Ta)$, $II_C(Ta)$, $III_A(Ta)$, and $III_B(Ta)$, respectively. The peak $II_A(Ta)$ is resolved only in the high-dose sample data while $II_B(Ta)$ and $II_C(Ta)$ are present in the high-, medium-, and low-dose data; $III_A(Ta)$ again is only resolved for the high dose while $III_B(Ta)$ appears in both high and medium dose. The position of $III_B(Ta)$, furthermore, is strongly dose-dependent and the temperature quoted above for this peak is for high dose. The Nb slope diagrams exhibit four substages centered at 26, 58, 94, and 134°K. These are labelled $II_A(Nb)$, $III_A(Nb)$, $III_B(Nb)$, and $III_A'(Nb)$, respectively. $II_A(Nb)$, $III_A(Nb)$, and $III_B(Nb)$ are all resolved in both the high- and medium-dose data, while $III_A'(Nb)$ only can be seen for high dose. The position of $III_B(Nb)$ is dose-dependent and the temperature quoted again refers to high dose.

The following peaks show first-order annealing characteristics insofar as their position appears to be dose-independent: $II_A(Ta)$, $II_B(Ta)$, $II_C(Ta)$, $II_A(Nb)$, and $III_A(Nb)$. The activation energies can be calculated from the equation

$$E = kT_c \left(1 - \frac{\Delta}{2T_c}\right) \left\{ \ln \left[\nu t \left(\frac{\rho_c}{\rho_F} \right)^{\gamma-1} \right] - \ln \left[\exp \left(\frac{E\Delta}{kT_c^2} \right) - 1 \right] \right\}, \quad (1)$$

where k is Boltzmann's constant, ρ_F is the specific resistivity of Frenkel defects, T_c is the temperature at the center of the peak on the derivative plots, ρ_c is the damage remaining at the beginning of the anneal at T_c , γ is the order of the reaction, ν is the frequency factor, and t is the pulse time. Equation (1) follows from the assumptions that Δ , the temperature interval between successive anneals, is constant over the peak and small compared to the width of the peak, and that t is small enough that $\Delta\rho/\rho_c$ for any one anneal is much less than 1. $\Delta\rho$ is the amount recovered in the particular pulse. Under the conditions of the experiment, we have for first order

$$E \approx kT_c \ln \nu t. \quad (2)$$

The frequency factor ν has been calculated from the

TABLE II. Damage rate data.

Sample	Total damage ($10^{-2} \mu\Omega \text{ cm}$)	Damage rate [$10^{-26} \mu\Omega \text{ cm} / (e/\text{cm}^2)$]
II (Ta)	2.56	
VI (Ta)	8.85	2.95±0.30
VII (Ta)	3.19	
I (Nb)	3.88	
V (Nb)	12.0	3.86±0.40

TABLE III. First-order substages in Nb and Ta.

Peak	T_c (°K)	ν (10^{11} sec $^{-1}$)	E_{act} (eV)	$\Delta\rho_{peak}/\Delta\rho_{tot}$ (%)
II _A (Ta)	23.0±1.5	4.8	0.065	8.4
II _B (Ta) high dose	49.0±1.5	10.2	0.14	8.4
II _B (Ta) med. dose	49.5±1.5	10.3	0.14	8.7
II _B (Ta) low dose	51.5±1.5	10.7	0.14	10.7
II _C (Ta) high dose	66.0±1.5	13.7	0.19	6.4
II _C (Ta) med. dose	66.0±1.5	13.7	0.19	5.8
II _C (Ta) low dose	65.0±1.5	13.5	0.19	5.4
II _A (Nb) high dose	25.5±2.5	5.3	0.075	16.4
II _A (Nb) med. dose	29.0±2.5	6.11	0.075	19.7
III _A (Nb) high dose	59.0±2.5	12.3	0.16	24.1
III _A (Nb) med. dose	57.5±2.5	12.0	0.16	27.6

expression

$$h\nu = kT, \quad (3)$$

where h is Planck's constant and T is the temperature. Activation energies for the peaks listed above, together with the percent of damage that has annealed out within each particular substage, are shown in Table III. III_A(Ta) is tentatively identified as a first-order substage, but, because it is only resolved in the high-dose data and is relatively weak, no further analysis will be attempted for III_A(Ta).

Two peaks, III_B(Ta) and III_B(Nb), show higher-order characteristics. An exact second-order kinetics

was assumed and the annealing data were plotted for the high and medium doses on an Arrhenius diagram. The results for Ta high and medium doses are shown in Fig. 6 while Nb high and medium doses are shown in Fig. 7. The linearity is reasonably good over almost three decades in all cases. Activation energies can readily be calculated from the slopes. Furthermore, the intercept of the curve with the horizontal axis can be used to find an approximate value of ν/ρ_F . These results are tabulated in Table IV together with T_0 , the temperature corresponding to the intercept, and the percent annealing within the substages. A check on the consistency of assuming second-order kinetics can now be made by solving for the order from the expression for the dose-

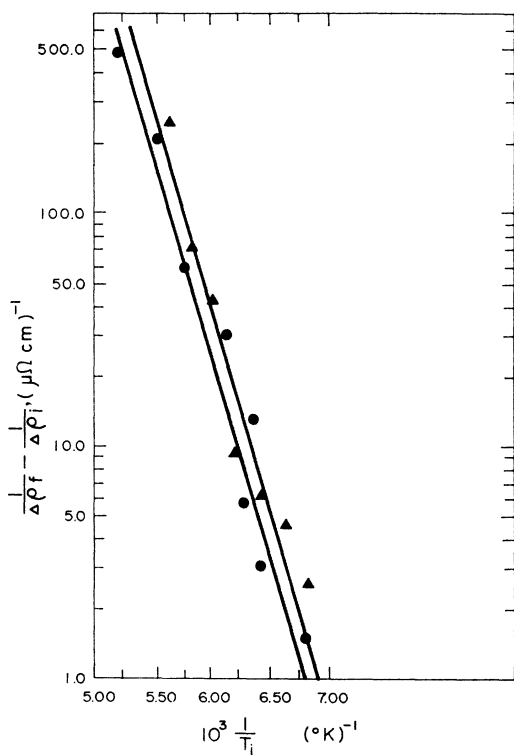


FIG. 6. Arrhenius plots for high- and medium-dose Ta. Circles and triangles denote high and medium dose, respectively.

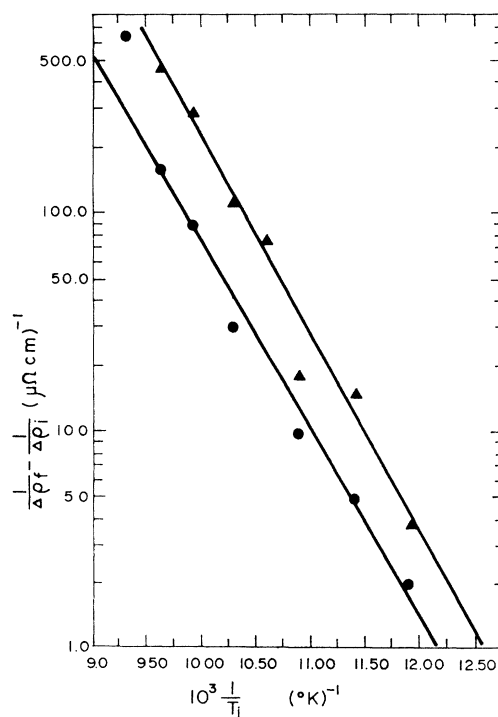


FIG. 7. Arrhenius plot for high- and medium-dose Nb. Circles and triangles denote high and medium dose, respectively.

TABLE IV. Arrhenius plot analysis of second-order peaks in Ta and Nb.

Peak	E_{act} (eV)	T_0 (°K)	ν/ρ_F [(sec $\mu\Omega$ cm) $^{-1}$]	$\frac{\Delta\rho_{peak}}{\Delta\rho_{tot}}$ %
III _B (Ta)	0.33±0.02	146	4.17×10 ⁸	30.8
high dose	[0.32±0.02] ^a			
III _B (Ta)	0.33±0.03	144	4.17×10 ⁸	34.5
med. dose	[0.31±0.03] ^a			
III _B (Nb)	0.16±0.02	82	5.28×10 ⁷	13.6
high dose	[0.16±0.02] ^a			
III _B (Nb)	0.18±0.03	80	5.28×10 ⁷	19.5
med. dose	[0.17±0.03] ^a			

^a Values in brackets are calculated from Eq. (4).

dependent peaks shift. An approximate expression for the activation energy for γ greater than 1 can readily be written as

$$E \approx kT_c \ln[\nu t(\rho_c/\rho_F)^{(\gamma-1)}]. \quad (4)$$

If we consider two similar processes with different defect concentrations, an expression for the temperature shift can be derived using Eq. (4) such that

$$\Delta T_{12} \approx (\gamma-1)(k/E)T_{c1}T_{c2} \ln(\Delta\rho_{c2}/\Delta\rho_{c1}), \quad (5)$$

where ΔT_{12} is the temperature shift and subscripts 1 and 2 refer to the two doses. Experimental values for T_{1c} , T_{2c} , ΔT_{12} , $\Delta\rho_{c2}/\Delta\rho_{c1}$, and calculated values for γ are listed in Table V. Thus substages III_B(Ta) and III_B(Nb) apparently obey second-order kinetics within experimental error. Finally, Eq. (4), with $\gamma=2$, can be used to recalculate the activation energies. These values are shown in brackets in Table IV.

TABLE V. Dose dependence of second-order peaks in Ta and Nb.

Substage	T_{1c} (°K)	T_{2c} (°K)	ΔT_{12} (°K)	$\Delta\rho_{c2}$ ($\mu\Omega$ cm)	$\Delta\rho_{c1}$ ($\mu\Omega$ cm)	n_{calc}
III _B (Ta)	174.5	167.0	7.5	2.90×10 ⁻²	1.10×10 ⁻²	2.0 ±0.15
III _B (Nb)	99.5	94.5	5.0	1.63×10 ⁻²	0.76×10 ⁻²	1.95 ±0.20

TABLE VI. Summary of recovery model.

Stage	Ta				Nb				Process
	Substage	Temp. (°K)	Order	E_{Act} (eV)	Substage	Temp. (°K)	Order	E_{Act} (eV)	
I	I _A (Ta)	9 ⁽¹⁾⁻⁽³⁾	N.D.	[0.03] ^a	I _A (Nb)	15 ⁽¹⁾⁻⁽³⁾	N.D.	[0.03] ^a	Close-pair and free migration of type-A interstitials
	I _B (Ta)	15 ⁽¹⁾⁻⁽³⁾	N.D.	[0.03] ^a					
II	II _A (Ta)	23.0	First	0.065	II _A (Nb)	26.5	First	0.075	Type-A interstitial release from traps
	II _B (Ta)	51.0	First	0.14					
	II _C (Ta)	65.0	First	0.19					
III	II _A (Ta)	123	N.D.	N.D.	III _A (Nb)	58.0	First	0.16	Close-pair and free migration of type-B interstitials
	III _B (Ta)	165-175	Second	0.32	III _B (Nb)	90-100	Second	0.17	
III'					III' _A (Nb)	135	N.D.	N.D.	Type-B interstitial release from traps

^a Numbers in brackets have been estimated.

V. DISCUSSION

A. First-Order Stages in Ta and Nb

Recent work by Burger *et al.*¹ and by Hemmerich *et al.*³ shows annealing substages at 9 and 15°K for Ta and at 15°K for Nb. These substages are not present in the work reported in this article because the irradiation was carried out at approximately 14°K. However, they will be taken into account in this discussion.

From the reported characteristics of the low-temperature peaks at 9 and 15°K in Ta, it is plausible to assign the recovery of an interstitial defect, which we shall label as type A, to these substages. Doping experiments on Ta show^{1,3} that oxygen in concentration of 1×10^{-3} clearly depresses the peak at 15°K while the annealing in Ta between 20 and 120°K is strongly enhanced. It is proposed that a similar model explains the recovery of Nb for the 15°K substage and the annealing between 20 and 50°K. Thus, the substages II_A(Ta), II_B(Ta), and II_C(Ta) are interpreted as showing the release of type-A interstitials from impurity sinks and subsequent annihilation with vacancies. Some retrapping and cluster formation may also take place. For Nb, the peak II_A(Nb) is given the same interpretation. As supporting evidence, it may be noted that these states are virtually nonexistent in pure Ta but become dominant upon doping.³ Furthermore, all of these stages are much too broad to signify single processes for both Ta and Nb. This is reasonable since one would expect a range of binding energies for different impurities and different interstitial-impurity configurations.

It remains to be explained why the damage production curves in the present work and those presented in the earlier work by El-Salam and DeFord² show linearity

to a fractional-defect concentration of roughly 1×10^{-4} even though the irradiation was performed at a temperature which in both metals was approximately equal to that of a free migration peak. Irradiation at a temperature above a close-pair peak clearly will not interfere with the linearity in the damage production since close-pair annihilation is independent of defect and impurity concentration. Furthermore, if the impurity concentration at all times during the damage production is much larger than the concentration of free vacancies, the damage production will be approximately linear because the free migration state will be suppressed to a large extent. (Thus, the nonlinearity should be small for the present impure samples.) This interpretation is supported by the fact that doping pure Ta with oxygen to a concentration of 1×10^{-3} depresses the recovery below 20°K from 40 to 5%.³

There are two more first-order peaks to be considered, namely, III_A(Ta) and III_A(Nb). In accordance with a two-interstitial model, III_A(Ta) is tentatively identified as the close-pair recovery peak for a second type of interstitial which we shall call type B. This peak has been observed in previous experiments¹⁻³ and shows little dependence on impurity concentration. III_A(Nb) is harder to identify. It appears in the annealing spectrum as a broad substage with possibly multiple superimposed spikes. It could either be the type-B interstitial close-pair recovery substages forming a broad peak, or the type-A interstitials being released from traps. Further studies comparing pure and doped samples are necessary to make a decision.

B. Second-Order Stages in Ta and Nb

In Sec. IV it was shown that substages III_B(Ta) and III_B(Nb) were strongly dose-dependent and that III_B(Ta) obeys second-order kinetics for the whole substage. III_B(Nb) obeys second order for a little more than the lower one-half; the subsequent high-temperature tail may signify either a competing process or a tendency toward higher orders of kinetics. About 20% of the total damage remains in the high-dose samples after these second-order peaks. Several mechanisms that could account for these features were examined. The most plausible model points toward free migration of the type-B interstitial with subsequent interstitial-vacancy annihilation and impurity trapping as the processes giving rise to these substages.

This model was considered in some detail. The processes can be described by a set of differential-rate equations⁵ that can be readily combined to give

$$dv/dt = K_i [1 - (K_{iT}\tau/K_i v) \ln(v_0/v)]^2 v^2, \quad (6)$$

where v and τ are the concentrations of free vacancies and traps, respectively. v_0 is the initial concentration

of free vacancies at the start of the stage. K_i and K_{iT} are the rate constants for free migration resulting in annihilation and trapping, respectively. Equation (6) can be interpreted as a second-order rate equation with a variable-rate constant. Initially, when $v_0 \approx v$, the second term in the brackets is much smaller than one and the kinetics is second order. Then, as v becomes smaller, the second term in the rate constant may become comparable to 1 and the order will steadily rise above 2. This clearly depends on the magnitude of $(K_{iT}/K_i)(\tau/v)$ versus $\ln(v_0/v)$. At the end of the stage, $dv/dt=0$, so that

$$1 - \frac{K_{iT}\tau}{k_i v_F} \ln\left(\frac{v_0}{v_F}\right) = 0, \quad (7)$$

where v_F is the final concentration of free vacancies. From the annealing curves we may estimate v_0/v_F for Ta and Nb, if the simplifying assumption is made, that the resistivity contribution of a trapped interstitial is the same as that of a free one:

$$v_0/v_F(\text{Ta}) = 2.25, \quad v_0/v_F(\text{Nb}) = 1.25.$$

Assuming that $K_{iT}/K_i \approx 1$, we can calculate τ in terms of v_0 for both materials as follows:

$$\tau(\text{Ta}) = 0.55v_0(\text{Ta}) \quad \text{and} \quad \tau(\text{Nb}) = 3.6v_0(\text{Nb}).$$

Assuming that $\rho_F(\text{Ta}) \approx \rho_F(\text{Nb})^b$ and that $v_0(\text{Ta}) \approx v_0(\text{Nb})$, one may conclude that the concentration of impurity traps is about seven times greater for Nb than for Ta. Referring back to the resistance ratios for the samples in question, it is striking to note that the residual resistivity is approximately seven times greater for Nb than for Ta— $[\rho_{295^\circ\text{K}}(\text{Ta}) \approx \rho_{295^\circ\text{K}}(\text{Nb})]$. Using the calculated values⁷ for $\rho_F(\text{Ta})$ and $\rho_F(\text{Nb})$, we can estimate v_0 for the Ta and Nb high-dose samples to be

$$v_0(\text{Ta}) = \Delta\rho_0(\text{Ta high dose})/\rho_F(\text{Ta}) = 2.3_0 \times 10^{-4},$$

$$v_0(\text{Nb}) = \Delta\rho_0(\text{Nb high dose})/\rho_F(\text{Nb}) = 1.1_5 \times 10^{-4},$$

where $\Delta\rho_0$ is the damage remaining at the start of the type-B interstitial free-migration peak. The effective concentrations of impurity traps are then equal to

$$\tau(\text{Ta}) = 1.2_5 \times 10^{-4} \quad \text{and} \quad \tau(\text{Nb}) = 4.5_0 \times 10^{-4}.$$

From the resistivity-ratio measurements, we determined that for the high-dose samples

$$\Delta\rho_0(\text{Ta})/\rho_0(\text{Ta}) = 0.7 \quad \text{and} \quad \Delta\rho_0(\text{Nb})/\rho_0(\text{Nb}) = 0.1,$$

where ρ_0 is the residual preirradiation resistivity at 11.5°K. From these ratios one can readily compute the average specific resistivity due to the impurity sinks, where ρ_{imp} is the specific resistivity due to impurities since

$$\rho_F v_0 = (\Delta\rho_0/\rho_0)\rho_{\text{imp}}\tau.$$

⁵ H. H. Neely, D. W. Keefer, and A. Sosin, Phys. Status Solidi **28**, 675 (1968).

⁶ P. G. Lucasson and R. M. Walker, Phys. Rev. **127**, 485 (1962).

⁷ G. Youngblood, S. Myhra, and J. W. DeFord, following paper, Phys. Rev. **188**, 1101 (1969).

The results are

$$\bar{\rho}_{\text{imp}}(\text{Ta}) = 4.9_5 \mu\Omega \text{ cm/at.}\%$$

and

$$\bar{\rho}_{\text{imp}}(\text{Nb}) = 1.4_5 \mu\Omega \text{ cm/at.}\%$$

These values are somewhat higher than typical values noted in the literature ($2\text{--}3 \mu\Omega \text{ cm/at.}\%$).⁸ The reason could be that only a fraction of the total impurity concentration is effective as sinks. The annealing procedure during the sample preparation could also have led to impurity precipitation resulting in large $\bar{\rho}_{\text{imp}}$ values. This would be more pronounced for the relatively impure Nb samples than for the Ta samples.

Note that because Nb has the greatest concentration of impurities it shows more suppression of the free-migration stage III_B(Nb). This stage also features a high-temperature tail indicating that the last one-third of the recovery within this stage obeys an order of kinetics greater than 2, in agreement with Eq. (6).

The annealing curve for the Nb high-dose sample indicates a peak at about 134°K. This substage III_{A'}(Nb) is tentatively identified as type-B interstitial release from impurity sinks. The data, however, are too uncertain to warrant any further discussion of this peak.

Finally, we may speculate as to the identity of the two types of interstitials believed to be responsible for the annealing spectra of Ta and Nb. Extensive computer calculations on interstitials and vacancies in α -Fe have been done by Johnson.⁹ He notes, in accord with Erginsoy *et al.*,¹⁰ that the $\langle 110 \rangle$ -split interstitial has the minimum-energy configuration. The $\langle 111 \rangle$ -split interstitial, or crowdion, on the other hand, was found to have a very shallow local-minimum energy configuration. Finally, the $\langle 100 \rangle$ -split interstitial was found to be unstable. Migration energies for the $\langle 110 \rangle$ and the $\langle 111 \rangle$ interstitials were estimated to be 0.33 and 0.04 eV, respectively. From Table IV, the activation energy for free migration of the type-B interstitial in

Ta is 0.32 eV. Furthermore, the energy for free migration of the type-A interstitial at 15°K in Ta may be estimated as about 0.03 eV from simple temperature scaling considerations. The close agreement may be fortuitous since we are comparing two different metals, but it is plausible to adopt the $\langle 111 \rangle$ -split interstitial as type A and the $\langle 110 \rangle$ -split interstitial as type B.

VI. CONCLUSION

The annealing spectra for Ta and Nb show impurity-dependent substages for Ta in the temperature range 20–120°K and for Nb in the temperature range 20–50°K. The positions of these substages do not depend on defect density. These substages are interpreted as release of $\langle 111 \rangle$ -split interstitials from traps.

A second type of interstitial, tentatively identified as the $\langle 110 \rangle$ -split interstitial, migrates at 95°K in Nb and at 170°K in Ta, and gives rise to substages obeying apparent second-order kinetics. There may be associated close-pair recovery peaks centered at 123°K in Ta and 60°K in Nb. The temperature positions of the free-migration states are dose-dependent.

Detailed calculations, based on an interstitial trapping model for stage-III free migration, give at least qualitative agreement with the observed characteristics.

There is evidence for the $\langle 110 \rangle$ -split interstitial release from traps in Nb giving rise to a substage at 135°K.

The above assignment and the associated activation energies in Ta are consistent with the computer calculations of Johnson in Fe.

The proposed model for recovery up to 285°K in electron-irradiated Nb and Ta is summarized in Table VI.

ACKNOWLEDGMENTS

The authors wish to express their gratitude to all members of the Radiation Damage Group at the University of Utah for their help on the project. In particular, they are indebted to Gerald Youngblood for his assistance during the run. In addition, a special thanks goes to Dr. Abraham Sosin for his critical reading of the manuscript and many helpful discussions.

⁸ J. O. Linde, *Ann. Physik* **14**, 353 (1932); **15**, 219 (1932).

⁹ R. A. Johnson, *Phys. Rev.* **134**, A1329 (1964).

¹⁰ C. Erginsoy, G. H. Vineyard, and A. Englert, *Phys. Rev.* **133**, A595 (1964).